Magnesium based tin-silicon alloys under pressure: first-principles evolution search results

Yuri V. Luniakov

Institute of Automation and Control Processes of the Far Eastern Branch of the Russian Academy of Sciences, Vladivostok, Russia

luniakov@mail.ru

ABSTRACT The search of minimal enthalpy structures of ternary magnesium alloys of different stoichiometry $Mg_xSi_ySn_z$ under pressure $P \leq 6$ GPa has been performed using the software suite USPEX implementing the evolution algorithm combined with the density functional theory (DFT) approach. The evolutionary search has yielded new possible ternary compounds of the stoichiometries $Mg_{12}Si_3Sn$, Mg_4SiSn and Mg_6Si_3Sn, which have negative enthalpy of formation at pressures in the range of 0 to 10 GPa and which are not substitution solutions. These compounds have metallic properties and formation energies comparable to those of binary silicides Mg_xSi_y.

1. Introduction

Due to their promising properties such as high melting point [1], small size of the forbidden zone, environmental safety and sufficient cheapness compared to thermoelectrics based on bismuth, tellurium and lead, e.g. Bi_2Te_3 [2], PbTe and PbSn [3], semiconductor magnesium silicides and stannides are very interesting materials. They are very effective for infrared detection due to their high electrical conductivity and ability to absorb light in the infrared region of the spectrum. All of these properties allow these materials to be widely used as thermal elements in industrial production [4–8], as infrared detectors in optical fibers [9], and for use in hydrogen energy technologies [10].

Regarding the research on magnesium silicides, only the pressure-stabilized Si-rich phases, like $MgSi_2$, Mg_5Si_6, $MgSi$ and Mg_9Si_5 can form near the interface Mg_2Si/Si [11, 12]. Two relatives of Mg_2Si, namely Mg_9Si_5 and Mg_5Si_6, have been experimentally observed in the supersaturated solid solution of Al–Mg–Si [13]. Two phases of this solution, i.e., the β' and β" phases, have been resolved and are considered to correspond to the hexagonal P6$_3$/m phase of Mg_9Si_5 [14, 15] and the monoclinic C2/m phase of Mg_5Si_6 [16, 17], respectively. Huan et al. [11, 12] discovered that Mg_2Si is nearly equivalent to Mg_9Si_5 from 6 to 24 GPa based on the first principles investigation of high-pressure phases of Mg_2Si. Stable compounds of magnesium with tin and germanium are much more difficult to make, so the only known structures are Mg_2X, where X is Sn and Ge. It is even more complicated to obtain stable compounds for the ternary systems of different stoichiometry than $Mg_2Si_{1-x}Sn_x$ and $Mg_2Si_{1-x}Ge_x$. At present, there are only experimental data on solid solutions of the composition $Mg_2Si_{1-x}Sn_x$ and $Mg_2Si_{1-x}Ge_x$.

Besides binary stannides and magnesium silicides, their mixed compounds Mg_2XY (where X, Y = Si, Sn, Ge) are also of interest, as they have rather unique thermoelectric properties compared to the corresponding binary compounds. Some experimental results suggest [18] that solid solutions of $Mg_2Si_{1-x}Sn_x$ show better thermoelectric performance when n-type doping is used. For example, three-component alloys of composition $Mg_2Si_{0.35}Sn_{0.65}$ and $Mg_2Ge_{0.25}Sn_{0.75}$ are characterized by lower thermal conductivity and higher figure of merit due to mixing of different components and high carrier mobility [19–21]. Solid solutions of the composition $Mg_2Si_{0.4}Sn_{0.6}$ have promising thermodynamic properties [22, 23] due to the overlap and degeneracy of the valence bands of Si and Sn, which leads to an increase in the effective mass of electrons [24, 25]. These properties make mixed compositions of Mg_2X potentially interesting materials for thermoelectric applications.

Changes in the thermal conductivity of $Mg_2Si_{1-x}Sn_x$ silicon-tin alloys can also occur when their stoichiometry is altered due to the presence of various defects and impurities in them. This is due to the lack of complete solubility in the $Mg_2Si_{1-x}Sn_x$ and $Mg_2Ge_{1-x}Sn_x$ systems [1]. Several attempts to improve the thermal conductivity have been made by

modifying the structure of alloys by doping. To study the thermoelectric properties of $Mg_2Si_{1-x}Sn_x$, many theoretical and experimental investigations have been carried out [26–28] in order to determine the most effective alloying elements and to evaluate the influence of internal and external defects.

However, the properties of the three-component alloys $Mg_xSi_ySn_z$ for all possible stoichiometries have not yet been investigated [29]. At present, only data on solid solutions of the compositions $Mg_2Si_{1-x}Sn_x$ and $Mg_2Si_{1-x}Ge_x$ are available. This implies that only the structure of antifluorite with symmetry $Fm\overline{3}m$ is considered in the calculation of the structures of stannidosilicides, since the silicide and magnesium stannide Mg_2Si and Mg_2Sn have this structure. In besides the silicides, application of evolutionary search methods to the calculations of Mg_2Si, Mg_2Sn and Mg_2Ge allowed us to reproduce the known phase transitions from antifluorite to anticottunite and Ni_2In-type structures and to predict unknown structures of the silicide Mg_2Si [30], Mg_2Sn [31] and Mg_2Ge [32] at high pressures. This gives hope for new results for $Mg_xSi_ySn_z$ alloys of arbitrary stoichiometry. The aim of this work is to search for optimal structures of the three-component system $Mg_xSi_ySn_z$ using modern evolutionary methods [33] and to study the stability of these structures under normal pressure conditions and zero temperature as well as under pressures from 0 to 10 GPa.

2.   Methodology of calculation

For evolutionary modeling of the three-component Mg–Si–Sn system, Universal Structure Predictor: Evolutionary Xtallography (USPEX) algorithms were applied in the variable composition mode [33–37]. Details of the evolutionary search algorithms can be found in the reviews [37, 38]. During the evolutionary search, from 40 to 60 generations of structures were produced depending on the convergence, which was considered to be achieved when the most energetically favorable structure remained unchanged for 20 consecutive generations. Each generation contained 20 structures and the first generation contained more than 120 structures, with 4 to 32 atoms per every structure. The convex hull obtained from the calculations contained structures of 6 – 10 atoms each with very few exceptions as shown below in the next section (see Table 1). The structures of the first generation were randomly selected from the list of 230 space groups. In the following generations, 50 % of the lowest-energy structures were inherited from the previous generation, 10 % of the structures were produced by lattice mutation, 10 % of the structures were obtained by atom transmutation, and the remaining 30 % of the structures were generated randomly.
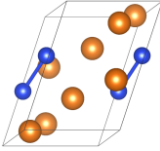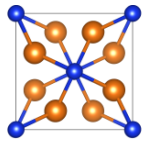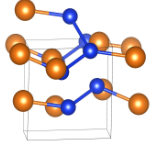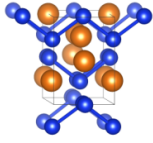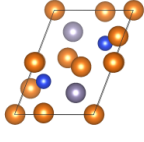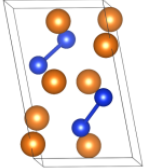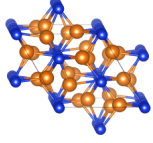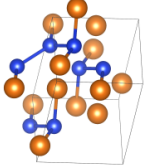
All USPEX generated structures were then relaxed using the conjugate gradient method implemented in the VASP software [39] with an energy precision of up to 0.1 meV per cell. The one-electron wave functions were expanded using a plane-wave basis with a kinetic energy cutoff of $E_{cut} = 500$ eV; the exchange-correlation potential in the Purdue–Burke–Ernzerhof parameterization [40] was used in the generalized gradient approximation. The valence electron states of the Mg, Si and Sn atoms are $2p^63s^2$, $3s^23p^2$ and $3s^23p^22d^{10}$, respectively. The Brillouin zones were sampled using a Monkhorst–Pack mesh with k-points resolution of $\pi \times 0.1$ Å^{-1}. Atomic positions were optimized until the convergence was achieved in the force of $\sim 10^{-3}$ eV/Å and in the energy of $\sim 10^{-6}$ eV. The dependence of the relative energies of the studied structures on a kinetic energy cutoff and the density of the k-point mesh was investigated and found to have no significant influence on entropy difference.
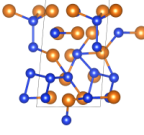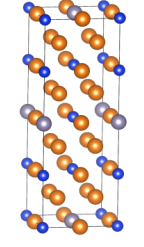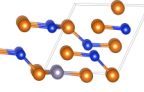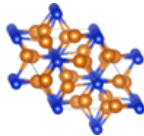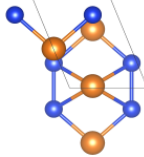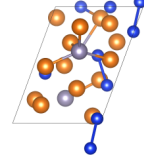
3.   Results and discussion

More than ten thousand negative enthalpy magnesium based tin-silicon alloys $Mg_ASi_BSn_C$ at pressures from 1 to 6 GPa were obtained by evolutionary searching. The projections of $Mg_ASn_BSi_C$ structure formation enthalpies to the ternary Mg_2Si–Si–Sn plot is shown in Fig. 1, the color of each symbol on which is determined by the value of the distance in eV/atom to the ternary convex hull. The warmer the color, the more the structure deviates from the convex hull, which is the most stable configuration, colored deep blue. This increased distance from the most stable arrangement corresponds to a reduction in the overall structural stability of the crystal lattice. The unstable crystal structures with positive enthalpies are shown in gray.

Enthalpy of formation for the three-component system $Mg_ASi_BSn_C$ can be defined as $E_F = [E(Mg_ASi_BSn_C) - (AE_{Mg} + BE_{Si} + CE_{Sn})]/(A+B+C)$, where A, B, C are the number of magnesium, silicon, and tin atoms; E_{Mg}, E_{Si}, are E_{Sn} their formation energies in the normal (crystalline) states, respectively. For each pressure, USPEX calculations automatically determine the optimal structure of silicon, diamond, and magnesium silicide, that can be used in formation enthalpy calculations of multicomponent structures. For silicon and tin, only a third of all calculations yielded the correct diamond-like structure, while the rest of calculations yielded structures with higher enthalpy and wrong symmetry, such as $P6_422$ (181 space group) for silicon and $P6_3/mmm$ (194 space group) for tin. The e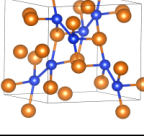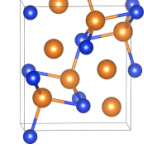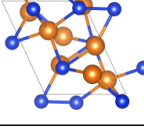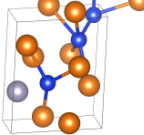nergy difference between the structure obtained in this way and the structure in the ground state does not exceed 0.001 eV/atom for silicon and 0.04 eV/atom for tin. The structure of magnesium was not determined during the evolutionary search, only the structure of its silicide Mg_2Si has been obtained. To calculate the enthalpy of all structures obtained in this work, the enthalpies of the known ground-state structures of Mg [41–43], Si [41] and Sn [44, 45] at investigated pressures were used as a reference for the formation enthalpy calculations. The reference crystalline structures at the ambient pressure conditions were taken from the on-line databases [34, 46, 47]. For magnesium, this structure is a hexagonal close packed structure of 194 space group symmetry $P6_3/mmc$, while for silicon and tin it is a diamond-like cubic structure b-tin $Fd\overline{3}m$ of 227 symmetry group.

Table 1: Structures, corresponding to the vertices of the convex hull at pressures of 6, 4, 2, 1 and 0.025 GPa. The brackets in the first column of the table indicate the total number of atoms in the unit cell. On the unit cell shown in the last column Si atoms are represented by small blue spheres, Mg atoms by large yellow spheres, and Sn atoms by large gray spheres.

Pressure/ composition	Lattice parameters						Symmetry	$E_{\text{formation}}$, eV/atom	Unit cell
	a, Å	b, Å	c, Å	a, °	β, °	γ, °			
6 GPa, Mg_4Si (10 atoms)	5.28	7.42	5.32	76.86	76.98	71.65	P-1 (2)	−0.042	
6 GPa, Mg_2Si (6 atoms)	6.49		5.09	90	90	90	I4/mcm (140)	−0.098	
6 GPa, MgSi (8 atoms)	5.19	5.39	5.25	68.67	89.25	100.15	P-1 (2)	−0.113	
6 GPa, Mg_3Si_4 (14 atoms)	13.75	3.57	5.07	90	90	90	Imm2(44)	−0.080	
6 GPa, Mg_4SiSn (12 atoms)	5.03	7.14	7.58	71.67	76.64	106.78	P-1 (2)	−0.137	
4 GPa, Mg_2Si (12 atoms)	5.30	8.28	5.12	90	90	100.95	P21(4)	−0.073	
4 GPa, Mg_3Si_2 (10 atoms)	7.720	7.235	6.643	90	90	104.5	C2/c (15)	−0.108	
4 GPa, MgSi (8 atoms)	5.736	5.330	5.362	84.53	111.57	112.68	P-1 (2)	−0.075	

|									
4 GPa, Mg_7Si_5 (24 atoms)	10.5	7.08	7.05	60.19	79.08	77.05	P1 (1)	−0.087	
4 GPa, $Mg_{12}Sn_3Si$ (16 atoms)	6.12	6.12	17.24	90	90	90	I4/mmm (139)	−0.144	
4 GPa, Mg_6Si_3Sn (10 atoms)	7.06	4.18	7.279	90	114.3	90	Pm(6)	−0.095	
2 GPa, Mg_3Si_2 (10 atoms)	7.41	7.41	12.16	90	90	120	R-3C(167)	−0.087	
2 GPa, Mg_2Si (6 atoms)	5.67	10.14	4.07	90	90	90	I(mmm) (71)	−0.046	
2 GPa, Mg_7Si_2Sn (20 atoms)	9.49	7.50	7.88	75.12	111.12	118.41	P1 (1)	−0.063	
1 GPa, Mg_3Si_2 (20 atoms)	8.21	8.66	5.94	90	110.40	90	P21/c(14)	−0.040	
1 GPa, Mg_2Si (12 atoms)	6.99	4.17	8.01	90	90	90	Pnma(62)	−0.115	
0.025 GPa, Mg_2Si (12 atoms)	5.68	7.42	7.20	70.72	73.87	107.88	P-1 (2)	−0.024	
0.025 GPa, Mg_6Si_3Sn (10 atoms)	5.41	6.52	6.29	75.63	98.64	97.77	P1 (1)	−0.060	
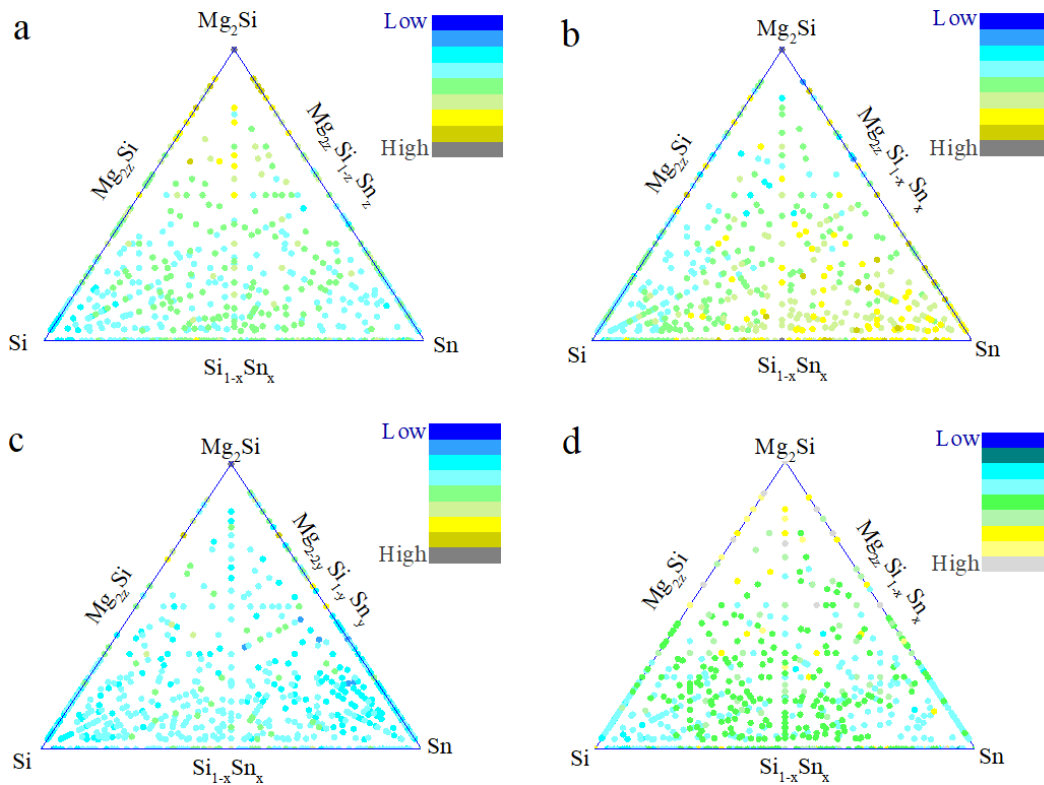
FIG. 1. The ternary composition-formation enthalpy phase diagram of the $Mg_A Si_B Sn_C$ at pressures: 1 GPa (a), 2 GPa (b), 4 GPa (c), and 6 GPa (d). Each structure is colored according to the distance from the convex hull in eV/atom, which varies from blue minimum to dark gray (maximum) see the legend bar on the left. As the color of a crystal structure becomes more dark, the crystal structure is the less stable and further away from the convex hull

As can be seen in Fig. 1, the number of stable compounds of magnesium, tin and silicon is strongly dependent on both the pressure and the enthalpy of formation of these structures. Thus, if at 6 GPa we have more than a hundred structures with negative enthalpy of formation, at 4 GPa there are less than thirty, at 2 GPa there are twelve, and at 1 GPa there are only three. There are too few three-component systems that are stable at ambient pressure conditions, most of them are two-component ones.

Table 1 shows the lattice parameters and enthalpies of formation of the most stable compounds of magnesium, silicon and tin obtained by evolutionary methods at external hydrostatic pressures of 1, 2, 4 and 6 GPa. The largest number of stable structures is found at pressure $P = 6$ GPa. The convex hull at this pressure is formed by four binary silicides Mg_4Si, Mg_2Si, $MgSi$, Mg_3Si_4 and one ternary compound, which has the composition Mg_4SiSn and the symmetry P-1. The corresponding unit cells are shown in the last column of Table 1. The tin-silicon alloy Mg_4SiSn (2 symmetry group) is a solid solution with a triclinic unit cell in which Ge and Si atoms are uniformly distributed throughout the volume. Binary silicides at pressure $P = 6$ GPa are characterized by a wide range of stoichiometry, symmetry and composition from 80 % of Mg and 20 % of Si (Mg_4Si), to 43 % of Mg and 57 % of Si (Mg_3Si_4). If we compare the enthalpy of formation of ternary alloy Mg_4SiSn and binary silicides Mg_xSi_y, it turns out that at a pressure of 6 GPa, the ternary alloy Mg_4SiSn is about 0.02 eV more stable than the monosilicide MgSi 2 symmetry group P-1 and 0.04 eV more stable than the disilicide Mg_2Si 140 symmetry group I4/mcm.

At pressure $P = 4$ GPa, the convex hull is formed by four binary silicides MgSi, Mg_2Si, Mg_3Si_2, Mg_7Si_5 and two three-component alloys Mg_6Si_3Sn and $Mg_{12}Si_3Sn$. Binary silicides exhibit different symmetry and structure, which can be compared to corresponding silicides in open access databases [41, 46, 47] as will be shown later. The ternary alloy Mg_6Si_3Sn at pressure $P = 4$ GPa has an enthalpy of formation $E \sim -0.1$ eV and it forms crystal structure of group 6 symmetry (Pm). As shown in the last column of Table 1, the ternary compound Mg_6Si_3Sn comprises alternating Mg–Sn–Mg–Si and Mg–Si layers. In each mixed Mg–Sn–Mg–Si type layer one Sn or Si atom is bonded to two Mg atoms, with the bond length of Mg–Sn approximately 2.9 Å and the bond length of Mg–Si ranging from 2.6 to 2.8 Å. Similarly, in each Mg–Si type layer, one atom of Si is bonded to two atoms of Mg, with the bond length of the Mg–Si varying from 2.6 to 2.8 Å. The $Mg_{12}Si_3Sn$ compound has an enthalpy of formation $E = -0.144$ eV and consists of alternating layers of binary compounds Mg_2Si and Mg_2Sn. First, there is a layer of alternating MgSi and MgSn in this structure. Then there is a continuous layer of Mg atoms at 16 m Wyckoff position in the unit cell. Then there is a layer of MgSi silicide followed by a layer of Mg atoms. That is followed by a layer of alternating MgSi and MgSn and all repeats. The distance

between neighboring layers is equal to 2.155 Å. The alloy with stoichiometry $Mg_{12}Si_3Sn$ surprisingly turns out to be the most energetically favorable in the entire range of given pressures from 0 to 10 GPa.

At pressure $P = 2$ GPa, the convex hull is formed by two binary silicides Mg_2Si, Mg_3Si_2 and one ternary compound Mg_7Si_2Sn. The binary silicides Mg_2Si, Mg_3Si_2 have 71 and 167 space groups symmetry (Immm and R$\overline{3}$c), respectively. The three-component alloy Mg_7Si_2Sn has the lowest possible symmetry P1 and consists of Mg, Si and Ge atoms randomly distributed throughout the unit cell. The sustainability of this low symmetry structure remains questionable and requires further investigations. At pressure $P = 1$ GPa, the convex hull is formed only by two binary silicides Mg_2Si, Mg_3Si_2 of symmetry group 14 and 62 (P2$_1$/c and Pnma), respectively. At ambient pressure conditions, USPEX evolutionary searches found it difficult to identify stable three-component systems because most calculations tend to converge on two-component ones. There is only one ternary structure Mg_6Si_3Sn of 2 symmetry group P-1 at pressure $P = 0.25$ GPa, as shown at the end of Table 1.

For a more detailed study of the stability of the most energetically favorable structures in different pressures, all results presented in Table 1 were recalculated in the pressure range from 0 to 10 GPa with full geometry re-optimization. Fig. 2 shows the most stable structures with negative formation enthalpy, obtained by optimizing the results of the evolutionary search at each pressure in steps of 1 GPa. The most energetically favorable three-component alloy structure is three-component alloy $Mg_{12}Si_3Sn$ of 139 space group symmetry I4/mmm. This structure is the most stable of all obtained three-component ones. At pressures above 10 GPa, it loses enthalpy to a binary silicide Mg_3Si_2 of space group 15 symmetry, which has the lowest enthalpy of all binary silicides Mg_xSi_y obtained. The other two three-component structures Mg_6Si_3Sn and Mg_4SiSn are sufficiently higher in enthalpy than the $Mg_{12}Si_3Sn$ one. As shown in Fig. 2, it is also more stable than the trigonal structure of Mg_3Si_2 of symmetry group 167 (R-3c) in the entire pressure range below 10 GPa. Next on the Enthalpy-axis is the three-component structure Mg_6Si_3Sn, which is energetically more favorable than the binary silicide structure Mg_3Si_2 167 symmetry group only at pressures $P < 2$ GPa. At $P > 2$ GPa it loses to other structures, such as non-symmetric three-component alloy Mg_6Si_3Sn and binary silicide Mg_7Si_5. The Mg_7Si_5 structure looks defective and its stability remains questionable, as well as the stability of the non-symmetrical Mg_6Si_3Sn one.
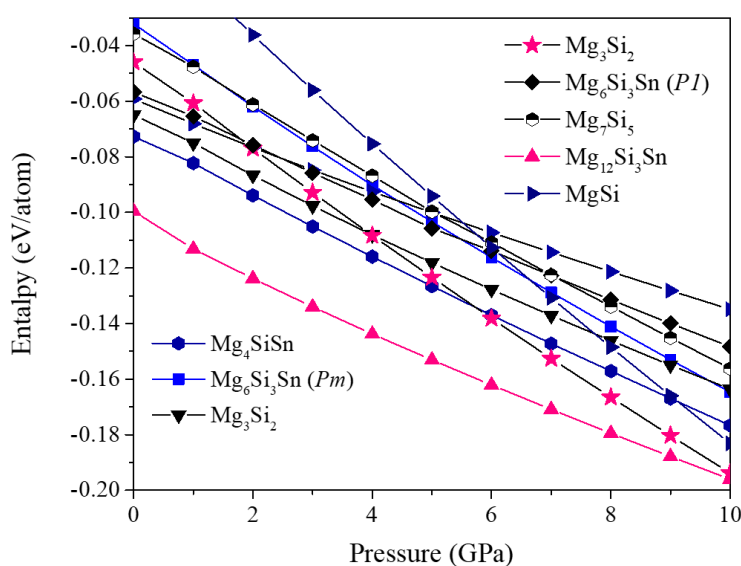

FIG. 2. Enthalpy-pressure dependence for the most energetically favorable crystal structures obtained by optimizing the results of the evolutionary search

Although this work is aimed at investigating ternary compounds, it is also useful to compare the obtained binary Mg_xSi_y compounds with the known results available in Material Project [41] and the Open Quantum Materials [46, 47] databases. Most were shared by our Vietnamese colleagues Huan et al., they are described in [11, 12].

The graph in Fig. 3 compares the enthalpy-pressure dependencies for known binary structures [41, 46, 47] with those obtained in the current study. The top two curves correspond to the most energetically favorable Mg_3Si_4 structures from the database [41] obtained by Huan et al. [11, 12]. We can see that their formation enthalpy is negative only for large non-zero pressures $P > 2$ GPa. Below, these two curves in Fig. 3 are the dark blue curve corresponding to the more energetically favorable Mg_3Si_4 structure obtained in the current study. This structure has the negative enthalpy of formation at any pressure $P \geq 0$. The binary silicide Mg_3Si_4 has 44 group symmetry Imm2 and the following lattice parameters: $a = 13.75$ Å, $b = 3.57$ Å, $c = 5.07$ Å, $\alpha = \beta = \gamma = 90°$.

Below, the curves discussed above are green curves with triangular symbols pointing upwards, corresponding to the structure of the monosilicide MgSi. The enthalpy values of this curve practically coincide with those of the curve obtained in the calculation of the most favorable MgSi structure from the database [41] in the whole pressure range
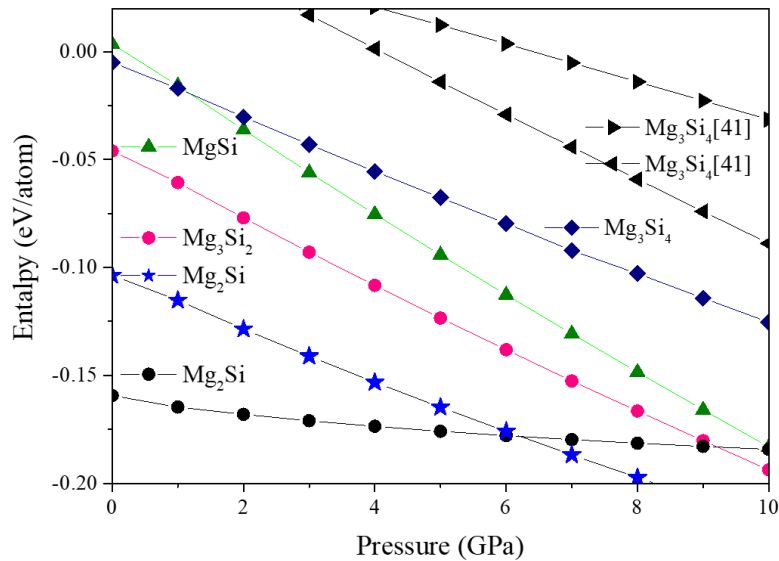
FIG. 3. Enthalpy-pressure dependence for the most stable binary magnesium silicides, obtained by evolutionary search, in comparison with the calculated enthalpy pressure-dependence of known structures

studied. If we plot the enthalpy-pressure dependence for the MgSi structure from the database [41] and then compare it with the dependence obtained for the triclinic MgSi structure in this work, their difference does not exceed 0.03 eV in the entire pressure $0 < P \leq 10$ GPa. The binary monosilicide MgSi has 2 group symmetry P-1 and the following lattice parameters: $a = 5.44$ Å, $b = 5.42$ Å, $c = 6.06$ Å, $\alpha = 110.7°$, $\beta = 113.8°$, $\gamma = 83.6°$. In this structure, there are three non-equivalent Mg atoms bonded to six Si atoms (see Table 1, last column).

The red curve with triangular symbols pointing down corresponds to the structure of Mg_3Si_2. As in the case of MgSi monosilicide, the curve practically coincides with the curve obtained in these calculations for the most energetically favorable Mg_3Si_2 structure. The possible difference is not more than 0.03 eV, which can be considered an acceptable error, making the curves for these structures practically indistinguishable. The Mg_3Si_2 structure with the lowest energy from [41] has 15 group symmetry C2/c and lattice parameters: $a = 7.82$ Å, $b = 7.30$ Å, $c = 6.87$ Å, with angles $\alpha = 90°$, $\beta = 104.26°$, $\gamma = 90°$ (see Table 1, last column). In the ambient pressure conditions, the Mg_3Si_2 structure, obtained in this work and shown in Fig. 3, has 15 group symmetry and lattice parameters $a = 8.09$ Å, $b = 7.38$ Å and $c = 6.63$ Å, and angle $\beta = 104°$, leading to an increase in unit cell volume of about 1 % compared to the data from [41]. Both of these structures are characterized by parallel-oriented silicon dimers with Si–Si bond lengths of approximately 2.4 Å. The enthalpy-pressure dependence for the structure in this work is practically identical to that obtained from the database structure [41] (see Fig. 2). The difference between them does not exceed 0.025 eV per atom in the pressure range from 0 to 10 GPa.

The Mg_2Si anticottunite-type structure obtained in this study (star-marked curve in Fig. 1) differs from the known antifluorite-type structure of Mg_2Si of symmetry group 225 (bullet-marked curve in Fig. 1). In the absence of external pressure, the energy difference between the structure obtained in this work and the known antifluorite-type structure is 0.056 eV and decreases to 0 at pressure around 6 GPa. Obviously, in this study a suboptimal anticottunite-type Mg_2Si structure has been obtained, which is more energetically favorable at high pressures $P > 6$ GPa [30]. It has 62 group symmetry Pnma and cell parameters $a = 7.04$ Å, $b = 4.20$ Å and $c = 8.05$ Å, which are close to the Material Project Pnma cell parameters $a = 6.99$ Å, $b = 4.14$ Å and $c = 7.99$ Å [41]. This difference in results might be caused by the use of the variable composition mode in the USPEX code [33–37], where for each fixed ratio of Mg, Si, Sn components a smaller number of structures is generated, which does not always allow finding the minimum energy structure.

Nevertheless, the results for ternary structures with other stoichiometries of Mg_4SiSn, Mg_6Si_3Sn, and $Mg_{12}Sn_3Sn$ demonstrate rather good stability with respect to their enthalpies. As shown in Fig. 2, besides two curves corresponding to the ternary compounds Mg_4SiSn and $Mg_{12}Sn_3Sn$, there are two curves corresponding to two different types of structures of the ternary compound Mg_6Si_3Sn. The first one is triclinic with 1 group symmetry P1 and the second one is monoclinic with 6 group symmetry Pm. The triclinic structure of Mg_6Si_3Sn (Table 1, last row) has an asymmetric cell with lattice parameters $a = 5.41$ Å, $b = 6.52$ Å, $c = 6.29$ Å, $\alpha = 75.63°$, $\beta = 98.64°$, $\gamma = 97.77°$, while the monoclinic structure of Mg_6Si_3Sn (Table 1 10 row) has two right angles $\alpha = \gamma = 90°$, one obtuse angle $\beta = 114.5°$ and lattice parameters $a = 7.29$ Å, $b = 4.26$ Å, $c = 7.42$ Å. The enthalpy difference for these two Mg_6Si_3Sn structures is no more than 0.01 eV at pressures $P \leq 1$ GPa and increases to ~ 0.02 meV with increasing pressure up to $P = 10$ GPa. At pressures $P \leq 2$ GPa, the triclinic structure is more stable, and at pressures $P > 2$ GPa, the monoclinic structure becomes more

enthalpy favorable. However, in order to draw conclusions about the stability of the obtained structures, it is also necessary to study their phonon spectra, which was done in this work.

To confirm the dynamical stability of three-component alloys, phonon dispersion curves at ambient pressure conditions have been calculated for Mg_4SiSn, $Mg_{12}Sn_3Si$ and two Mg_6Si_3Sn structures. The method of obtaining force constants from forces and atomic displacements using the $2 \times 2 \times 2$ supercells, developed by Togo A. and implemented in the PHONOPY code [48, 49], was used. As shown in Fig. 4, the phonon dispersion curves do not show any imaginary frequencies, which prove the stability of the corresponding compounds. Imaginary frequencies appear near the gamma points in the two graphs of the figure, imaginary frequencies appear only at the gamma points in the graphs of Fig. 4 (c and d), which is simply related to the size of the supercell used in the calculations. If it is too small, this leads to inaccurate force constants, which is the reason for the appearance of imaginary phonon frequencies [50]. To check the influence of size effects, additional calculations were performed with an enlarged $3 \times 3 \times 3$ supercell for Mg_6Si_3Sn, both triclinic and monoclinic. The results show that for monoclinic structure the imaginary frequencies disappear near the gamma point when the supercell size is increased, and the rest of the dispersion curves remain almost unchanged (see Fig. 4(e,f)). On the contrary, for triclinic structure, the negative dip near gamma point becomes deeper than for the $2 \times 2 \times 2$ supercell calculations which evidence the instability of the monoclinic structure in contrast to the triclinic one.
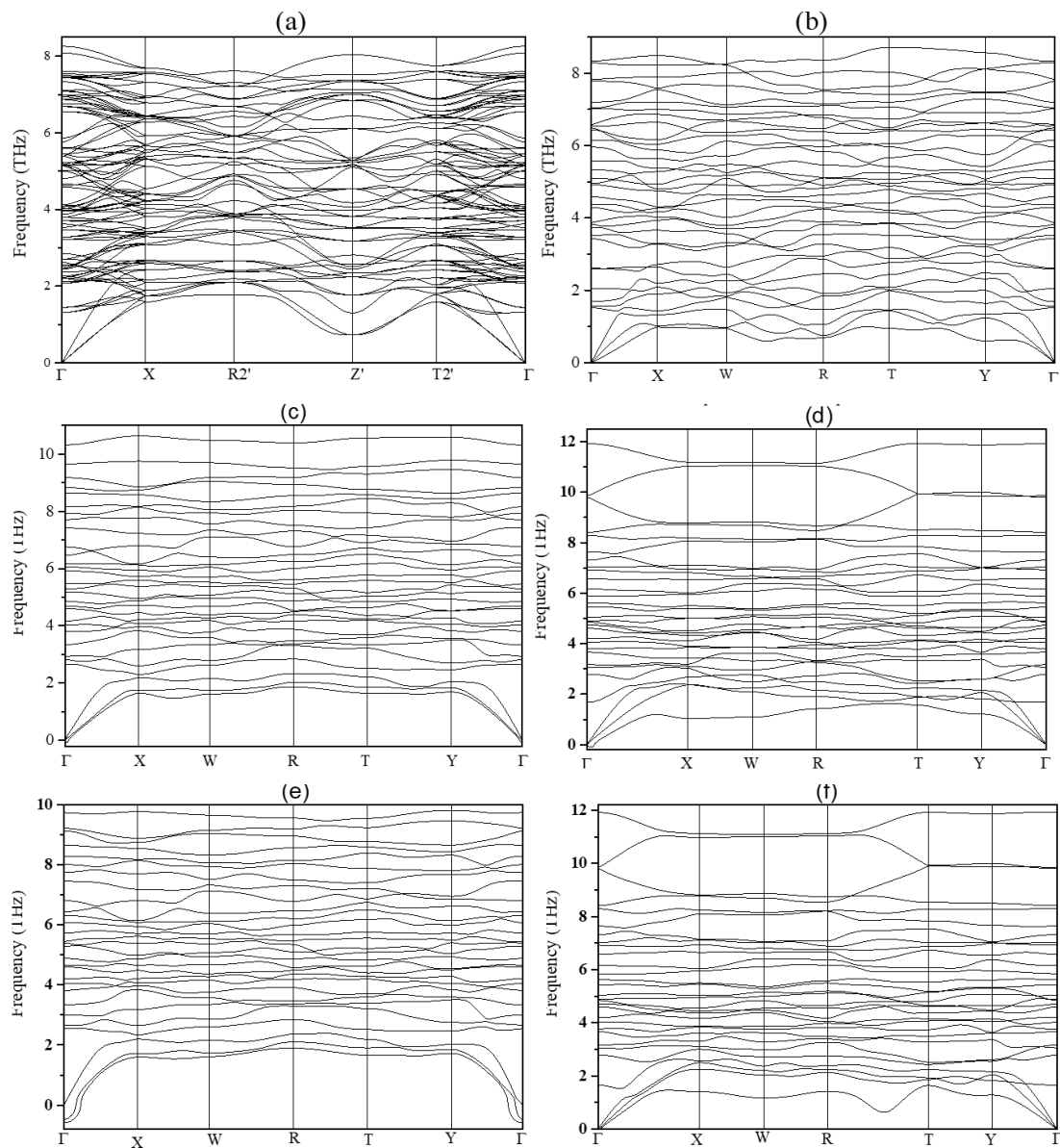
FIG. 4. Phonon dispersion curves of (a) $Mg_{12}Sn_3Si$; (b) Mg_4SiSn; (c) triclinic Mg_6Si_3Sn; (d) monoclinic Mg_6Si_3Sn; (e) triclinic Mg_6Si_3Sn obtained using the enlarged $3 \times 3 \times 3$ supercell; (f) monoclinic Mg_6Si_3Sn obtained using the enlarged $3 \times 3 \times 3$ supercell

Phonon structure calculations allow a simple estimation of the phonon contribution to the free energy

$$F_{\text{phonon}} = \frac{1}{2} \sum_{q,v} \hbar\omega_{q,\nu} + k_B T \sum_{q,v} \ln\left(1 - e^{-\frac{\hbar\omega_{q,\nu}}{k_B T}}\right),$$

where q denotes the wave vector, ν is the phonon band index, ω is the corresponding phonon frequency, T is the temperature, and k_B is the Boltzmann constant. The estimate shows that at temperatures $T \leq 350$ K, this contribution does not exceed 0.05 eV per atom in absolute value, and for different structures, this contribution is approximately the same value, their difference being less than 0.02 eV.

In order to investigate the conductive properties of three-component systems at ambient pressure conditions, densities of states were calculated for the most energetically favorable compounds $Mg_xSi_ySn_z$. Fig. 5 displays the electronic state densities of the three-component alloys with the lowest formation energy $Mg_{12}Si_3Sn$, Mg_4SiSn and Mg_6Si_3Sn. This information can be used to evaluate the conductive properties of the materials. All of the alloys considered above have states at Fermi levels indicating that they all exhibit metallic properties in one way or another unlike the binary silicide Mg_2Si and stannide Mg_2Sn, which are semiconductors under normal conditions [30–32]. However, from the magnitude of the density of states in Fig. 5, the best metallic properties are likely to be exhibited by the solid solutions of Mg_4SiSn (Fig. 5(a)) and $Mg_{12}Si_3Sn$ (Fig. 5(b)) stoichiometries, which has significantly more of them at the Fermi level.

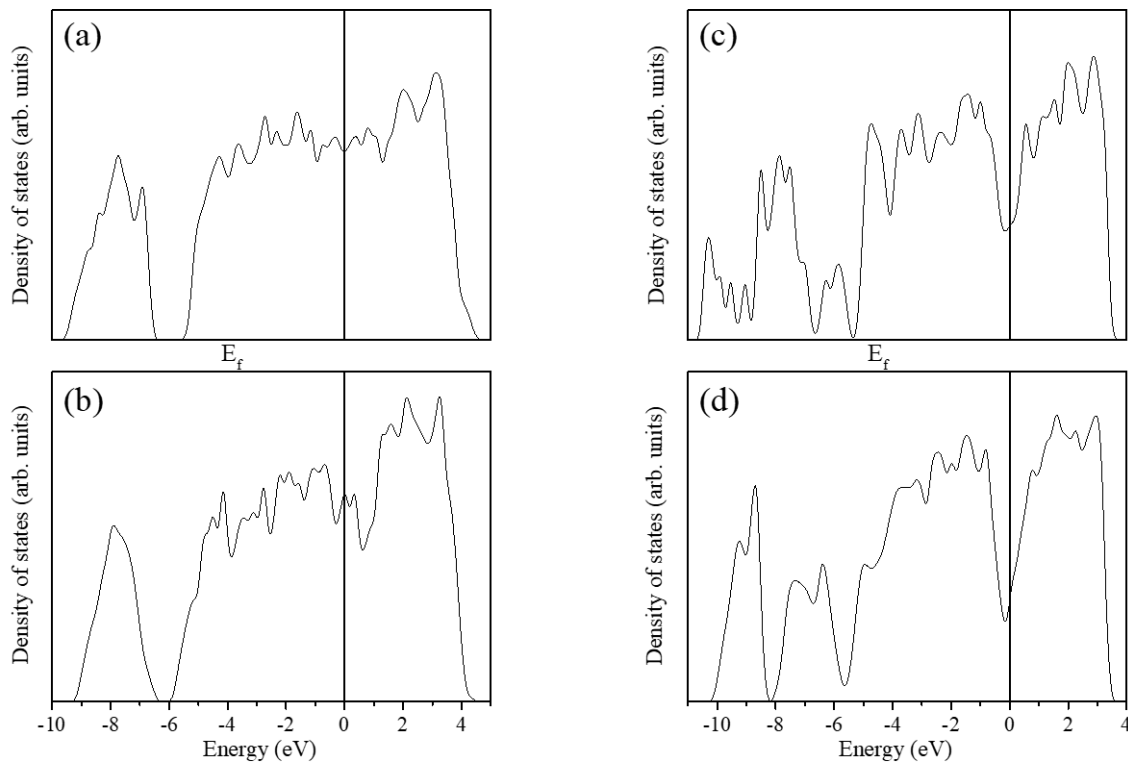FIG. 5. Density of electronic states of the most energetically favorable ternary compounds (a) Mg_4SiSn; (b) $Mg_{12}Sn_3Si$; (c) triclinic Mg_6Si_3Sn; (d) monoclinic Mg_6Si_3Sn. The Fermi level is chosen as the energy reference point

4. Conclusion

The results of the evolutionary modeling of three-component systems allowed to reproduce binary structures of the known stoichiometries $MgSi$ and Mg_3Si_2, as well as to obtain new structures of the stoichiometries Mg_4SiSn, Mg_6Si_3Sn, $Mg_{12}Sn_3Si$, and Mg_7Si_2Sn with the ternary alloy $Mg_{12}Si_3Sn$ being the most stable one. All of them have a negative enthalpy of formation, comparable to the enthalpy of formation of binary structures in the studied pressure range $0 < P \leq 10$ GPa. Phonon dispersion and density of states calculations confirmed the dynamical stability and metallic properties of the newly identified ternary alloys besides the triclinic structure. Density of states calculations indicate that the ternary alloys exhibit metallic properties, unlike the binary silicides and stannides.

References

[1] Nayeb-Hashemi A.A., Clark J.B. The Mg-Sn (Magnesium-Tin) system. *Bulletin of Alloy Phase Diagrams*, 1984, **5** (5), P. 466–476.

[2] Yamashita O., Tomiyoshi S. Effect of annealing on thermoelectric properties of bismuth telluride compounds. *Jpn J. Appl. Phys.*, 2003, **42** (2R), 492.

[3] Marfoua B., Lagoun B., Lidjici H., Benghia A., Gueddouh A. Theoretical investigation of structural, electronic and thermoelectric properties of p-n type $Mg_2Si_{1-x}Sn_x$ system. *Pramana J. Phys.*, 2020, **94** (1), 6.

[4] Liu W., Tan X., Yin K., Liu H., Tang X., Shi J., Zhang Q. Convergence of conduction bands as a means of enhancing thermoelectric performance of n-type $Mg_2Si_{1-x}Sn_x$ solid solutions. *Phys. Rev. Lett.*, 2012, **108** (16), 166601.

[5] Sankhla A., Patil A., Kamila H., Yasseri M., Farahi N., Mueller E. and de Boor J. Mechanical alloying of optimized Mg2(Si,Sn) solid solutions: understanding phase evolution and tuning synthesis parameters for thermoelectric applications. *ACS Appl. Energy Mater.*, 2018, **1** (2), P. 531–542.

[6] LeBlanc S., Yee S.K., Scullin M.L., Dames C., Goodson K.E. Material and manufacturing cost considerations for thermoelectrics. *Renew. Sustain. Energy Rev.*, 2014, **32**, P. 313–327.

[7] Gaultois M.W., Sparks T.D., Borg C.K.H., Seshadri R.K., Bonificio W.D., Clarke D.R. Data-driven review of thermoelectric materials: performance and resource considerations. *Chemistry of Materials*, 2013, **25** (15), P. 2911–2920.

[8] de Boor J., Dasgupta T., Mueller E. Thermoelectric properties of magnesium silicide-based solid solutions and higher manganese silicides. In *Materials Aspect of Thermoelectricity*, CRC press, Boca Ration, USA, 2016, 160 p.

[9] Vantomme A., Mahan J.E., James G.L., Margriet P.B., Bael V., Temst K., Haesendonck C.V. Thin film growth of semiconducting Mg_2Si by codeposition. *Appl. Phys. Lett.*, 1997, **70** (9), P. 1086–1088.

[10] Zhu Y., Han Zh., Jiang F., Dong E., Zhang B.-P., Zhang W., Liu W. Thermodynamic criterions of the thermoelectric performance enhancement in Mg_2Sn through the self-compensation vacancy. *Mater. Today Physics*, 2021, **16** (1), 100327.

[11] Huan T.D. Pressure-stabilized binary compounds of magnesium and silicon. *Phys. Rev. Mater.*, 2018, **2** (2), 023803.

[12] Huan T.D., Tuoc V.N., Le N.B., Minh N.V., Woods L.M. High-pressure phases of Mg_2Si from first principles. *Phys. Rev. B*, 2016, **93** (9), 094109.

[13] Huan T.D., Tuoc V.N., Le N.B., Minh N.V., Woods L.M. Characterizing magnesium-silicon binaries in Al-Mg-Si supersaturated solid solution by first-principles calculations. *J. Sci.-Adv. Mater. Dev.*, 2016, **1** (4), P. 527–530.

[14] Vissers R., Huis M.A., Jansen J., Zandbergen H.W., Marioara C.D., Andersen S.J. The crystal structure of the β' phase in Al–Mg–Si alloys. *Acta Mater.*, 2007, **55** (11), P. 3815–3823.

[15] Ravi C., Wolverton C. First-principles study of crystal structure and stability of Al–Mg–Si–(Cu) precipitates. *Acta Mater.*, 2004, **52** (14), P. 4213–4227.

[16] Zandbergen H.W., Andersen S.J., Jansen J. Structure determination of Mg_5Si_6 particles in Al by dynamic electron diffraction studies. *Science*, 1997, **277** (5330), P. 1221–1225.

[17] Andersen S.J., Zandbergen H.W., Jansen J., Traeholt C., Tundal U., Reiso O. The crystal structure of the β-phase in Al–Mg–Si alloys. *Acta Mater.*, 1998, **46** (9), P. 3283–3298.

[18] Gao H., Zhu T., Liu X., Chen L., Zhao X. Flux synthesis and thermoelectric properties of eco-friendly Sb doped $Mg_2Si_{0.5}Sn_{0.5}$ solid solutions for energy harvesting. *J. Mater. Chem.*, 2011, **21** (16), P. 5933–5937.

[19] Zaitsev V.K., Fedorov M.I., Gurieva E.A., Eremin I.S., Konstantinov P.P., Samunin A.Y., Vedernikov M.V. Highly effective $Mg_2Si_{1-x}Sn_x$ thermoelectrics. *Phys. Rev. B*, 2006, **74** (4), 045207.

[20] Liu W., Tan X.J., Yin K., Liu H.J., Tang X.F., Shi J., Zhang Q.J., Uher C. Convergence of conduction bands as a means of enhancing thermoelectric performance of n-type $Mg_2Si_{1-x}Sn_x$ solid solutions. *Phys. Rev. Lett.*, 2012, **108** (16), 166601.

[21] Liu W., Kim H.S., Chen S., Jie Q., Lv B., Yao M., Ren Z., Opeil C.P., Wilson S., Chu Ch.-W., Ren Z. N-type thermoelectric material $Mg_2Sn_{0.75}Ge_{0.25}$ for high power generation. *Proc. Natl. Acad. Sci.*, 2015, **112** (11), P. 3269–3274.

[22] Zaitsev V.K., Fedorov M., Gurieva E.A., Eremin I.S., Konstantinov P.P., Samunin A., Vedernikov M.V. Thermoelectrics of n-type with ZT¿1 based on Mg_2Si–Mg_2Sn solid solutions. In: *ICP, 24th International Conference on Thermoelectrics*, Clemson, SC, USA, 2005, P. 204–210.

[23] Gao P., Berkun I., Schmidt R.D., Luzenski M.F., Lu X., Bordon Sarac P., Case E.D., Hogan T.P. Transport and mechanical properties of high-ZT $Mg_{2.08}Si_{0.4-x}Sn_{0.6}Sb_x$ thermoelectric materials. *J. Electron. Mater.*, 2014, **43**, P. 1790–1803.

[24] Tan J., Liu W., Liu H.J., Shi J., Tang X.F., Yin X.K., Zhang Q.J., Uher C. Multiscale calculations of thermoelectric properties of n-type $Mg_2Si_{1-x}Sn_x$ solid solutions. *Phys. Rev. B*, 2012, **85** (20), 205212.

[25] Dasgupta T., Stiewe C., de Boor J., Müller E. Influence of power factor enhancement on the thermoelectric figure of merit in $Mg_2Si_{0.4}Sn_{0.6}$ based materials. *Phys. Stat. Sol. A*, 2014, **211** (6), P. 1250–1254.

[26] Tobola J., Kaprzyk S., Scherrer H. Mg-vacancy-induced semiconducting properties in $Mg_2Si_{1-x}Sb_x$ from Electronic Structure Calculations. *J. Electron. Mater.*, 2010, **39**, P. 2064–2069.

[27] Kim S., Wiendlocha B., Jin H., Tobola J., Heremans J.P. Kim S., Wiendlocha B., Jin H., Tobola J., Heremans J.P. Electronic structure and thermoelectric properties of p-type Ag-doped Mg_2Sn and $Mg_2Sn_{1-x}Si_x$ ($x = 0.05, 0.1$). *J. Appl. Phys.*, 2014, **116** (15), 153706.

[28] Zhang L., Xiao P., Shi L., Henkelman G., Goodenough J.B., Zhou J. Suppressing the bipolar contribution to the thermoelectric properties of $Mg_2Si_{0.4}Sn_{0.6}$ by Ge substitution. *J. Appl. Phys.*, 2015, **117** (15), 155103.

[29] Kamila H., Sahu P., Sankhla A., Yasseri M., Pham H.N., Dasgupta T., Mueller E., de Boor J. Analyzing transport properties of p-type Mg_2Si–Mg_2Sn solid solutions: optimization of thermoelectric performance and insight into the electronic band structure. *J. Mater. Chem. A*, 2019, **7** (3), P. 1045–1054.

[30] Lunyakov Yu.V. Mg_2Si silicide under pressure: first-principles evolution search results. *Physics of the Solid State*, 2020, **62** (5), P. 880–884.

[31] Lunyakov Yu.V. Mg_2Sn stannide under pressure: first-principles evolutionary search results. *Physics of the Solid State*, 2021, **63** (4), P. 590–594.

[32] Lunyakov Yu.V. Mg_2Ge germanide under pressure: first principle evolutionary search results. *Physics of the Solid State*, 2022, **64** (10), P. 1414–1419.

[33] Oganov A.R., Pickard C.J., Zhu Q., Needs R.J. Structure prediction drives materials discovery. *Nat. Rev. Mater.*, 2019, **4** (5), P. 331–348.

[34] Oganov A.R., Lyakhov O.A., Valle M. How evolutionary crystal structure prediction works – and why. *Acc. Chem. Res.*, 2011, **44** (3), P. 227–237.

[35] Lyakhov A.O., Oganov A.R., Stokes H.T., Zhu Q. New developments in evolutionary structure prediction algorithm USPEX. *Comp. Phys. Comm.*, 2013, **184** (4), P. 1172–1182.

[36] Oganov A.R., Ma Y., Lyakhov A.O., Valle M., Gatti C. Evolutionary crystal structure prediction as a method for the discovery of minerals and materials. *Rev. Mineral. Geochem.*, 2010, **71** (1), P. 271–298.

[37] Oganov A.R. *Modern methods of crystal structure prediction*. John Wiley & Sons, USA, New York, 2011, 274 p.

[38] Oganov A.R., Glass C.W. Crystal structure prediction using ab initio evolutionary techniques: Principles and applications. *J. Chem. Phys.*, 2006, **124** (24), 244704.

[39] Kresse G., Furthmuller J.E. Efficient iterative schemes for ab initio total-energy calculations using a plane-wave basis set. *Phys. Rev. B*, 1996, **54** (16), P. 11169–11186.

[40] Perdew J.P., Burke K., Ernzerhof M. Generalized gradient approximation made simple. *Phys. Rev. Lett.*, 1996, **77** (18), P. 3865–3868.

[41] Jain A., Ong Sh.P., Hautier G., Wei Ch., Richards W.D., Dacek S., Cholia Sh., Gunter D., Skinner D., Ceder G., Persson K.A. The materials project: a materials genome approach to accelerating materials innovation. *APL materials*, 2013, **1** (011), 011002.

[42] Olijnyk H., Holzapfel W.B. High-pressure structural phase transition in Mg. *Phys. Rev. B*, 1985, **31** (7), 4682.

[43] Errandonea D., Meng Y., Husermann D., Uchida T. Study of the phase transformations and equation of state of magnesium by synchrotron x-ray diffraction. *J. Phys.: Condens. Matter*, 1989, **15** (8), 1277.

[44] Desgreniers S., Vohra Y.K., Ruoff A.L. Tin at high pressure: An energy-dispersive X-ray-diffraction study to 120 GPa. *Phys. Rev. B*, 2012, **39** (14), P. 10359–10361.

[45] Salamat, Ashkan, et al. High-pressure structural transformations of Sn up to 138 GPa: Angle-dispersive synchrotron X-ray diffraction study. *Phys. Rev. B*, 2013, **88** (10), 104104.

[46] Saal J.E., Kirklin S., Aykol M., Meredig B., Wolverton C. Materials design and discovery with high-throughput density functional theory: The Open Quantum Materials Database (OQMD). *JOM*, 2013, **65**, P. 1501–1509.

[47] Kirklin S., Saal J.E., Meredig B., Thompson A., Doak J.W., Aykol M., Ruhl S., Wolverton Ch. The Open Quantum Materials Database (OQMD): assessing the accuracy of DFT formation energies. *NPJ Comput. Mat.*, 2015, **1**, 15010.

[48] Togo A., Chaput L., Tadano T., Tanaka I. Implementation strategies in Phonopy and Phono3py. *J. Phys. Condens. Matter*, 2023, **35**, 353001-1-22.

[49] Togo A. First-principles phonon calculations with Phonopy and Phono3py. *J. Phys. Soc. Jpn.*, 2023, **92**, 012001-1-21.

[50] Lloyd-Williams J.H., Monserrat B. Lattice dynamics and electron-phonon coupling calculations using nondiagonal supercells. *Phys. Rev. B*, 2015, **92** (18), 184301.

Information about the authors:

Yuri V. Luniakov – Institute of Automation and Control Processes of the Far Eastern Branch of the Russian Academy of Sciences, Radio Str. 5, 690041, Vladivostok, Russia; luniakov@mail.ru